# Influence of the static atomic displacement on atomic resolution Z-contrast imaging

V. Grillo and E. Carlino*
*Laboratorio Nazionale TASC-INFM-CNR, Area Science Park, S. S. 14, Km 163.5, 34012 Trieste, Italy*

F. Glas
*Laboratoire de Photonique et de Nanostructures, CNRS, Route de Nozay, 91460 Marcoussis, France*
(Received 11 October 2007; revised manuscript received 23 November 2007; published 11 February 2008)

The influence of static atomic displacements, due to atomic size effects in alloys with atoms having different covalent or ionic radii, on high angle annular dark field image contrast is studied quantitatively by simulations and experiments. We show that the static displacements can have a large influence on the Z contrast, depending on the alloy composition and on the scanning transmission electron microscopy specimen thickness. This influence has to be taken into account for quantitative chemistry measurement based on Z-contrast imaging.

DOI: 10.1103/PhysRevB.77.054103 PACS number(s): 81.07.−b, 68.37.−d, 68.37.Lp

## I. INTRODUCTION

Scanning transmission electron microscopy (STEM) Z-contrast imaging is now well established as a powerful tool for studying the structural and chemical properties of solid-state matter at atomic resolution.[1] Indeed, the use of a high angle annular dark field (HAADF) detector allows the collection of the electrons scattered at high angle by the specimen nuclei, to form an incoherent image of the atomic columns seen along a high symmetry direction, with a resolution which can be better than 0.1 nm in modern instruments.[2] One of the main interests of the technique is that the positions of the projected atomic columns in the image depend only weakly on the microscope objective lens defocus and on the specimen thickness. This ensures that reliable structural information can be extracted from the raw image without having to compare the experimental results with time-consuming and delicate simulations, as is necessary for standard phase contrast high resolution transmission electron microscopy.[3] The HAADF image intensity $I$ depends sensitively on the average atomic number of the column, and important qualitative chemical information at atomic resolution can be achieved by direct inspection of the HAADF image contrast; this is why this method is also known as Z contrast.[3,4] Nevertheless, if quantitative information on the chemistry of the specimen is sought for, it becomes necessary to compare the experimental results with HAADF image simulations. In the past few years, several studies have endeavored to understand how to extract quantitative chemical information from HAADF images and to define methods for simulating these images.[5–9] Such attempts have to determine which parameters influence the image contrast and how to model their influence. Recently, a new method for atomic resolution quantitative chemical analysis based on HAADF imaging has been presented.[10] The method finds applications, in particular, in those cases where two or more alloys are present in the specimen and one of them, of known composition, may be taken as reference. This is the case, for example, when layers are grown on a known substrate. The method is based on the simulation of the HAADF image contrast of the alloys, in comparison with the contrast of the material of known composition, as a function of the composition and of the thickness of the STEM specimen. The influence of specimen thickness and objective lens defocus on the image contrast was already modeled in detail.[11,12] It is worthwhile to remark that the measurement of the image intensity is performed after the subtraction of the HAADF detector dark current; then the intensity is averaged in a volume comprising at least one lattice fringe spacing in the atomic resolution HAADF image. This approach is different with respect to what was reported by some authors in literature,[7] in which the difference between one maximum and one minimum is used for the quantification. This latter approach was used to overcome the problem that a quantification, based only on the intensity measured in the image maxima, is influenced by the presence of an additional background in the HAADF image. This additional background depends on the thickness and on the chemistry of the specimen, and influences both maxima and minima. Very likely, it is due to the finite size of the electron source and mechanical instabilities, which introduce a redistribution of intensity between maxima and minima.[11] In our approach, the average on a volume including at least one lattice fringe spacing makes the image intensity measurement independent of the additional background, producing an accurate quantification of the chemistry.[10] The comparison of the experimental result with sets of simulated results usually yields the composition of the specimen to within a few percent for the main constituents.

However, one effect that could strongly influence chemical quantification by HAADF imaging is the presence of static atomic displacements (SDs).[13] SDs occur in alloys which possess an average crystalline lattice, but where the atoms are actually displaced from the sites of the latter because they have different atomic or covalent radii. SDs have been known for a long time to induce modulations of the diffuse background in x-ray and electron diffraction patterns.[14] More recently, they have been shown to produce a typical fine scale diffraction contrast in the transmission electron microscopy (TEM) images of III-V semiconducting alloys.[15,16] The influence of the SDs due to an array of misfit dislocations on the HAADF image contrast has also been observed.[17,18] Finally, the effect of a random strain field on the HAADF image contrast has been considered.[19] However, the effect on the HAADF image contrast of SDs due to atomic size effects in alloys has not yet been considered.

 

In this work, we study quantitatively the influence of the SDs on the HAADF image contrast of alloys, concentrating on the case of III-V semiconducting materials. To this end, we simulate HAADF images of the $In_xGa_{1-x}As$ alloy for a range of In concentrations $x$, with and without including the SDs. The results show that the SDs can have a strong influence on the image contrast and that this influence depends on the composition and thickness of the specimen. By comparing the simulated images with experimental images of alloys of known composition, we demonstrate that the SDs must be taken into account whenever a measure of the composition of such specimens is derived from HAADF images.

## II. EXPERIMENT

The InGaAs alloy was chosen as a case material to investigate the effect of the SDs upon HAADF images because, in this material, the SDs have already been studied in detail by extended x-ray absorption fine structure,[20] electron diffraction,[21] and diffraction contrast TEM imaging.[16,22]

For simulation purposes, we first generate alloy supercells and then compute the HAADF images. To generate crystal supercells with SDs, we use the valence force field model[21,23–25] which is known to reproduce accurately the SD field in semiconductor alloys.[21] In the specific case of TEM, this model already proved successful as a basis for simulating the effects of the SDs on diffraction patterns,[16] channelled-electron-beam-induced x-ray emission,[26] diffraction contrast imaging (allowing to reproduce the fine structure of the two-beam dark field images of III-V alloys[21]), and structure factor calculation.[22,27] The HAADF images were calculated by multislice simulations in the frozen-phonon approach;[28] this method allows the most accurate simulation of the Z contrast.[29]

For the HAADF experiments, three quantum wells (QWs) of InGaAs alloys with different In concentrations were grown by molecular beam epitaxy on a (001) GaAs substrate.[30] The In compositions were measured by *in situ* x-ray photoelectron spectroscopy (XPS) and photoluminescence (PL).[30] The QWs had a maximum In concentration of 24% to ensure that they remained coherent with the GaAs substrate and free of interfacial dislocations that would introduce a further source of intensity variation in the HAADF images.[17] The STEM specimens were prepared in ⟨110⟩ cross-section geometry by mechanical grinding, ion milling, and final cleaning of specimen and specimen holder by a high-frequency low-energy plasma of $Ar_2$ and $O_2$.[31] The STEM HAADF experiments were performed on a JEOL 2010F microscope equipped with a field emission gun. The microscope objective lens has a measured spherical aberration coefficient $C_s=(0.47\pm0.01)$ mm, yielding a resolution of 0.13 nm in HAADF mode.[32] All the HAADF images were acquired by using an illumination convergence angle of 14 mrad and a detector collection angle of $84\leq 2\vartheta \leq 224$ mrad. The HAADF images were acquired in ⟨110⟩ zone axis orientation for different specimen thicknesses, which were measured by the projection method.[33,34]

Supercells, with and without SDs, were generated for In concentrations of 4%, 12%, 24%, 50%, and 75% in order to investigate the influence of different amounts of SDs. The HAADF image calculations were performed by using STEM_CELL software package, considering electron optical conditions pertaining to the corresponding STEM experiments. This software uses a parallel code to calculate the HAADF intensities with a very high accuracy, but allows a strong reduction in the computing time with respect to other approaches.[35,36] According to test simulations, and in agreement with published results,[37,38] 20 configurations are sufficient, in general, to converge to a precision better than 2% in simulating HAADF image contrast. This precision is improved if there are crystal symmetries in the unit cell. Whereas in the case of cells with SDs no exact symmetry can be found, in this study, the actual precision with 20 configurations was found to be better than 0.3%. This figure is the standard deviation from the average derived by repeating the calculations ten times on a selected supercell.

The supercells used for image simulation were extracted from large cells with SDs. The minimum requirement that the whole electron probe remains in the sample imposes supercells wider than 2 nm. In practice, each supercell is made of $6\times5$ nonequivalent unit cells. In fact, each InGaAs cell of the supercell is not equivalent to the other due to chemical fluctuation and SDs. The scattering potential and the probe were sampled on a $1024\times1024$ grid to fulfil the exact requirement for the maximum detector angle $\theta_{\max}$ of 224 mrad.[28] In fact, the size of the grid for the scattering potential requires: $\theta_{\max}<\min(N_{[1-10]}/3a_{[1-10]};N_{[001]}/3a_{[001]})\lambda$, where $N$ is the number of pixels in the chosen directions, $a$ is the relevant supercell size, and $\lambda$ is the electron wavelength. Cutting the $6\times5$ sample from the larger *ab initio* supercell produces an incorrect wrap around of the structure: the atoms at the borders then become artificially close. Whereas this is not a problem in a perfectly periodic cell, it might be the case when SDs are present; in particular, since it has been demonstrated that, in III-V alloys, the SDs are correlated over distances of several nanometers.[21] The justification for the use of reduced supercells is that the probe function intensity is negligible at the cell boundaries and that, for a large range of specimen thicknesses, the spreading of the probe to these regions remains small. This is true as long as the scanned region is selected only in the central part of the supercell. To test quantitatively the error involved in setting up this artificial boundary, an additional discontinuity in the SD field was created by swapping atomic columns in part of a supercell with an In concentration of 50%. As a result, at a distance of 0.5 nm from the discontinuity, the HAADF image intensity variation in the scanned area was less than 0.5%. In practice, for a typical supercell used in this work (2.4 nm along direction ⟨1−10⟩ and 3 nm along direction ⟨001⟩), the usable area was between 0.5 and 1.8 nm along direction ⟨1−10⟩, and between 0.6 and 2.4 nm along direction ⟨001⟩. In this rectangle made of $4\times3$ unit cells, a selection of $2\times2$, or in some cases $2\times1$ unit cells, was considered. A scan step of about 0.018 nm in each direction was set for a correct sampling: in this way, a $2\times2$ unit cell rectangle is sampled in a $48\times64$ pixel image. The resulting intensity was then averaged to obtain the intensity estimation for the relevant aver-

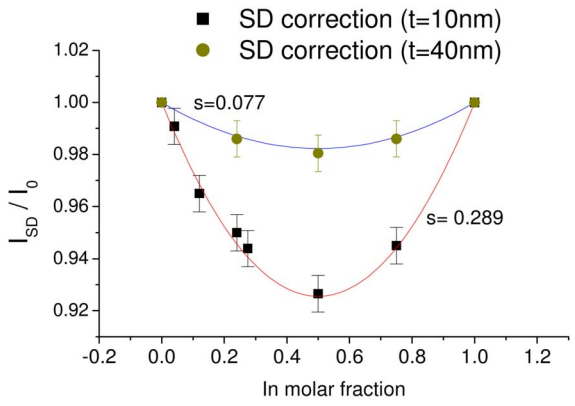


FIG. 1. (Color online) Ratio of the HAADF intensities calculated with and without including the effect of the SDs, as a function of the In atomic fraction, for two specimen thicknesses of 10 and 40 nm. The value $s$ of the fitting parameter with a parabola is also shown.

age composition. The comparison with the experimental images was performed on areas of the same size.

Different STEM specimen thicknesses were simulated. The thickness was varied from 0.4 up to 90 nm, with steps of 0.4 nm, for supercells with and without SDs. To reduce the computing time in the HAADF image calculations, a 10 nm thick supercell was repeated periodically along the beam direction up to the desired thickness. This again produces an artificial discontinuity in the SDs. To estimate the influence of this approximation, a 20 nm supercell was split in two parts, which were reassembled in inverted order, and the resulting cell was then turned upside down. This procedure permits to obtain a similar In distribution along the column (reducing the top bottom effect[10]) while at the same time creating an artificial discontinuity in the displacement field in the middle of the cell. The resulting intensity variation with respect to the standard calculation was only about 0.3%.

## III. RESULTS AND DISCUSSION

Figure 1 shows the ratio between the HAADF image intensities calculated with ($I_{SD}$) and without SDs ($I_0$), for specimen thicknesses $t$ of 10 and 40 nm. This ratio can be viewed as the multiplicative correction factor to be applied to the HAADF intensity calculated without SDs in order to take into account the effect of the SDs. Figure 1 shows that the effect of the SDs is largest for In concentrations around 50%, where the SDs are indeed maximum (on average). Our correction factor is well fitted by a parabolic law $I_{SD}/I_0 = 1 - s[x(1-x)]$, where $s$ is a fitting parameter (Fig. 1). Note that the SDs themselves[25,39] and the factors correcting the structure factors for the effect of the SDs[22,27] display a similar parabolic behavior as a function of the composition.

Figure 2(a) shows the HAADF intensity for the InGaAs alloy with an In concentration of 24% calculated with and without the effect of the SDs, together with the intensity calculated for the GaAs substrate, as a function of the specimen thickness. The curves in Fig. 2(a) are very close since

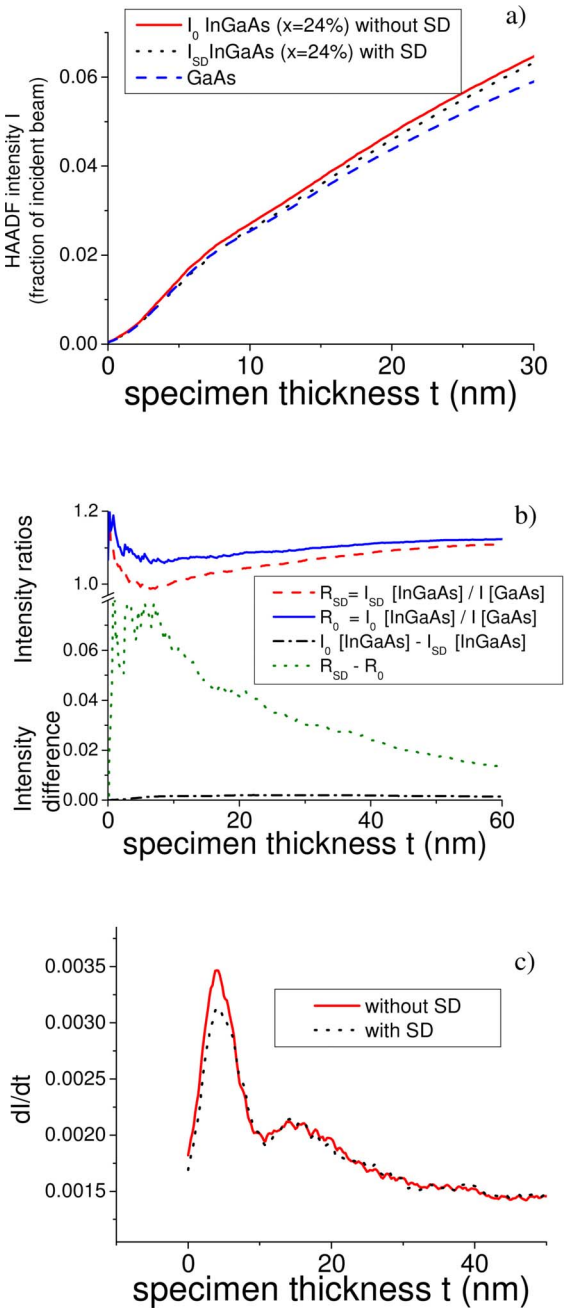


FIG. 2. (Color online) (a) HAADF intensity for an InGaAs alloy with In concentration of 24%, with and without considering the effect of the SDs, together with the calculated intensity for GaAs, as a function of the specimen thickness. (b) Starting from the top are reported: $R_0 = I_0(\text{InGaAs})/I(\text{GaAs})$, $R_{SD} = I_{SD}(\text{InGaAs})/I(\text{GaAs})$, $R_0 - R_{SD}$, and $I(\text{InGaAs}) - I_{SD}[(\text{InGaAs})$, respectively. (c) Derivative with respect to the specimen thickness of the HAADF intensity for the InGaAs alloy with 24% In concentration, as a function of the specimen thickness.

the correction for SDs is only a few percent of the HAADF intensity. However, it is essential to take this correction into account since it is of the same order as the difference between the intensities for the InGaAs alloy and the GaAs reference binary. This is shown quantitatively in Fig. 2(b) where four curves are reported as a function of the specimen

thickness: the first, in the bottom part, shows how the difference between $I$(InGaAs), with and without SDs effect, is nearly constant as a function of the sample thickness, whereas $R_0 = I_0(\text{InGaAs})/I(\text{GaAs})$, $R_{SD} = I_{SD}(\text{InGaAs})/I(\text{GaAs})$, and the difference $R_0 - R_{SD}$ depend sensitively on the specimen thickness. Hence, neglecting the role of SDs would induce large errors in the measurement of the In concentration by HAADF imaging as will be shown in the experiments below. Figure 2(c) shows the derivative with respect to the specimen thickness, of the HAADF intensity of the InGaAs alloy with 24% In concentration, as a function of the specimen thickness. This allows one to study the contribution of each successive slice of material encountered by the electron beam, which traverses the specimen. Figure 2(c) demonstrates that the effect of the SDs is mainly to offset the InGaAs HAADF image intensities by reducing the effect of electron channeling for specimen thicknesses below 10 nm, while leaving the contribution of the remaining slices almost unchanged.

Figure 3(a) shows a typical experimental low magnification high resolution HAADF image of the three InGaAs QWs grown on GaAs (001) substrate, along with the corresponding intensity line-profile taken perpendicularly to the interface. The image has been acquired by tuning the experimental conditions to achieve atomic resolution image, see Fig. 3(b) and then decreasing the magnification to display, at the same time, the three QWs along with the empty space where the dark counts of the detector can be measured and subtracted from the image. The experimental image directly indicates that the QWs have an increasing content of In, going from the GaAs substrate to the top of the epitaxial film, because the HAADF signal increases. The QWs have actual In concentrations of, respectively, $(5 \pm 1)\%$, $(12 \pm 1)\%$, and $(24 \pm 1)\%$, measured by XPS and PL as indicated above.[30]

Figure 3(c) shows the variation of the HAADF image intensity ratios $I_{\text{InGaAs}}/I_{\text{GaAs}}$ measured on the experimental images for each QW, as a function of specimen thickness (squares). Figure 3(c) also gives the intensity ratios calculated with (line) and without (dotted line) taking into account the SDs, by using our simulation procedure for alloy supercells with In concentrations of 5%, 12%, and 24%. We caution the reader that in the case of the In poor QW, the intensity was derived by interpolating the data obtained from a simulation performed on a supercell with an In concentration of 4%. Simulations with and without SDs all predict a dip of the $I_{\text{InGaAs}}/I_{\text{GaAs}}$ ratio around $t = 10$ nm, followed by a slow asymptotic rise to a constant value depending on the composition. Figure 3(c) clearly shows that a HAADF measure of the composition of the QWs seriously underestimates the In content if the effect of the SDs is ignored. This produces, in the worst of the considered cases, an absolute error of about 10% for the 24% In concentration. The main effect of the SDs is to increase the dip in the simulated intensity ratio. The deepening tends to decrease for large thicknesses, due to the normalization of the InGaAs intensities to the GaAs intensity, because the SDs correction to the intensity ratio itself vanishes at very high thickness (~100 nm). Taking into account the SDs produces a much better agreement between

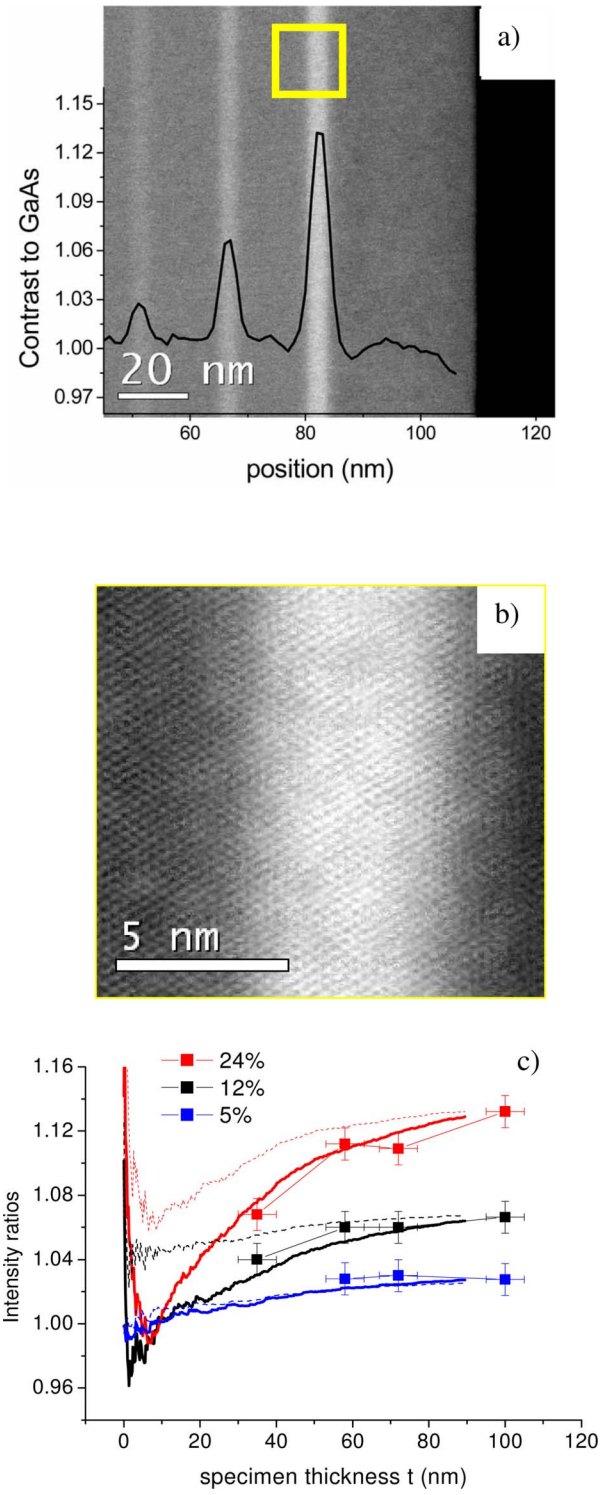


FIG. 3. (Color online) (a) Experimental low magnification high-resolution HAADF image, in ⟨110⟩ zone axis, of three QWs of InGaAs of known composition grown on GaAs (001) substrate, and corresponding intensity line profile. (b) High magnification high-resolution HAADF image corresponding to the region marked in (a). (c) Variation of the HAADF image intensity ratios $I_{\text{InGaAs}}/I_{\text{GaAs}}$ measured on the experimental image (squared dots with experimental errors) for each of the QWs, together with the expected intensity ratios calculated with (solid line) and without (dotted line) taking into account the SDs.

simulated and experimental curves. The improvement of the match between simulations and experiments is particularly evident for an In concentration of 24%, as this is the concentration where the SDs are largest among our three alloys. However, the improvement is also significant for the 12% and 5% concentrations. If the SD correction is not applied, the error in the evaluation of the In concentration increases with the latter. In particular, for specimen thickness of about 30 nm and In concentration of 24%, the error is as large as 10% in terms of absolute In concentration. For the same thickness, but for 5% In, the error is about 1%.

By using this result, we also estimate that the error made by not considering the SDs in our previous measurement of the Si concentration in GaAs:Si (Ref. 10) was actually below the other experimental uncertainties.

## IV. CONCLUSIONS

It has been demonstrated that SDs may considerably reduce the intensity in HAADF images of alloys, depending on specimen composition and STEM specimen thickness. Neglecting the SDs can introduce large errors in the measure of the specimen chemistry and it is, therefore, essential to take the SDs into account whenever HAADF images are used for quantitative purposes.

## ACKNOWLEDGMENTS

E. C. would like to thank A. Franciosi for the discussion at the origin of this work. V.G. thanks A. Rosenauer for the discussion about the idea of including SDs. The authors would also like to thank S. Rubini, G. Bais, A. Cristofoli, M. Piccin, F. Martelli, and A. Franciosi for providing the specimens; L. Palazzari and V. Rosato for the use of the parallel cluster of computers for the calculations and E. Cocianchich for the technical support.

*carlino@tasc.infm.it

[1] S. J. Pennycook and D. E. Jesson, Phys. Rev. Lett. **64**, 938 (1990).
[2] P. D. Nellist, M. F. Chisholm, N. Dellby, O. L. Krivanek, M. F. Murfitt, Z. S. Szilagyi, A. R. Lupini, A. Borisevich, W. H. Sides, Jr., and S. J. Pennycook, Science **305**, 1741 (2004).
[3] S. J. Pennycook, *Advances in Imaging and Electron Physics* (Academic, New York, 2002), Vol. 123, p. 140.
[4] E. Carlino, S. Modesti, D. Furlanetto, M. Piccin, S. Rubini, and A. Franciosi, Appl. Phys. Lett. **83**, 662 (2003).
[5] S. J. Pennycook, S. D. Berger, and R. J. Culberstone, J. Microsc. **144**, 229 (1986).
[6] C. P. Liu, A. R. Preston, C. B. Boothroyd, and C. J. Humphreys, J. Microsc. **194**, 171 (1999).
[7] D. O. Klenov and S. Stammer, Ultramicroscopy **106**, 889 (2006).
[8] S. C. Anderson, C. R. Birkeland, G. R. Anstis, and D. J. H. Cockayne, Ultramicroscopy **69**, 83 (1997).
[9] P. M. Voyles, D. A. Muller, and E. J. Kirkland, Microsc. Microanal. **10**, 291 (2004).
[10] E. Carlino and V. Grillo, Phys. Rev. B **71**, 235303 (2005).
[11] V. Grillo and E. Carlino, Ultramicroscopy **106**, 603 (2006).
[12] E. Carlino and V. Grillo, Arch. Metall. **51**, 23 (2006).
[13] T. G. Ramesh and S. Ramaseshan, Acta Crystallogr., Sect. A: Cryst. Phys., Diffr., Theor. Gen. Crystallogr. **27**, 569 (1971).
[14] B. E. Warren, B. L. Averbach, and B. W. Roberts, J. Appl. Phys. **22**, 1493 (1951).
[15] F. Glas, P. Hénoc, and H. Launois, in *Microscopy of Semiconducting Materials 1985*, edited by A. G. Cullis and D. B. Holt, IOP Conf. Proc. No. 76 (Institute of Physics, Bristol, 1985), p. 251.
[16] F. Glas, Phys. Rev. B **51**, 825 (1995).
[17] S. J. Pennycook and D. Nellist, *Impact of Electron Microscopy on Materials Research* (Kluwer Academic, Dordrecht, 1999), p. 161.
[18] D. D. Perovic, C. J. Rossouw, and A. Howie, Ultramicroscopy **52**, 353 (1993).
[19] Z. Yu, D. A. Muller, and J. Silcox, J. Appl. Phys. **95**, 3362 (2004).
[20] J. C. Mikkelsen, Jr. and J. B. Boyce, Phys. Rev. B **28**, 7130 (1983).
[21] F. Glas, C. Gors, and P. Hénoc, Philos. Mag. B **62**, 373 (1990).
[22] A. Rosenauer, M. Schowalter, F. Glas, and D. Lamoen, Phys. Rev. B **72**, 085326 (2005).
[23] P. N. Keating, Phys. Rev. **145**, 637 (1966).
[24] R. M. Martin, Phys. Rev. B **1**, 4005 (1970).
[25] M. Podgorny, P. M. Czyzyk, A. Balzarotti, P. Letardi, A. Kisiel, and M. Zimnal-Starnawska, Solid State Commun. **55**, 413 (1985).
[26] F. Glas and P. Hénoc, Philos. Mag. A **56**, 311 (1987).
[27] F. Glas, Philos. Mag. **84**, 2055 (2004).
[28] E. J. Kirkland, *Advanced Computing in Electron Microscopy* (Plenum, New York, 1998), p. 119.
[29] P. Xu, R. F. Loane, and J. Silcox, Ultramicroscopy **38**, 127 (1991).
[30] S. Rubini, G. Bais, A. Cristofoli, M. Piccin, R. Duca, C. Nacci, S. Modesti, E. Carlino, F. Martelli, A. Franciosi, G. Bisognin, D. De Salvaddor, P. Sciavuta, M. Berti, and A. V. Drigo, Appl. Phys. Lett. **88**, 141923 (2006).
[31] F. Capotondi, G. Biasiol, D. Ercolani, V. Grillo, E. Carlino, F. Romanato, and L. Sorba, Thin Solid Films **484**, 400 (2005).
[32] E. Carlino and V. Grillo, in *Proceedings of MCM VII Portoroze (SL) 2005*, edited by M. Che, G. Drazic, and S. Fidler (Slovene Society for Electron Microscopy, Ljubljana/Jozef Stefan Institute, Ljubljana, 2005), p. 159.
[33] D. B. Williams and C. B. Carter, *Transmission Electron Microscopy* (Plenum, New York, 1996), p. 630.
[34] V. Grillo and E. Carlino, in *Microscopy of Semiconducting Materials 2007*, edited by A. G. Cullis and P. A. Midgley, IOP Conf. Proc. (Institute of Physics, Bristol, in press).
[35] E. Carlino, V. Grillo, and P. Palazzari, in *Microscopy of Semiconducting Materials 2007* edited by A. Cullis and P. Midgley, IOP Conf. Proc. (Institute of Physics, Bristol, in press).

[36] V. Grillo and E. Carlino, in *Proceedings of MCM VII Portoroze (Sl) 2005*, edited by M. Che, G. Drazic, and S. Fidler (Slovene Society for Electron Microscopy, Ljubljana/Jozef Stefan Institute, Ljubljana, 2005).

[37] G. R. Anstis, S. C. Anderson, C. R. Birkenland, and D. J. H. Cockayne, Scanning Microsc. **11**, 287 (1997).

[38] C. Dwyer and J. Etheridge, Ultramicroscopy **96**, 343 (2003).

[39] V. Petkov and S. J. L. Billinge, Physica B **305**, 83 (2001).